Sacrificial Carbon Strategy toward Enhancement of Slurry Methanation Activity and Stability over Ni-Zr/SiO_2 Catalyst

Fanhui Meng,*,†,‡ Xin Li,† Greg M. Shaw,‡ Paul J. Smith,‡ David J. Morgan,‡ Michal Perdjon,‡ and Zhong Li*,†

†Key Laboratory of Coal Science and Technology of Ministry of Education and Shanxi Province, Taiyuan University of Technology, Taiyuan 030024, Shanxi, China

‡Cardiff Catalysis Institute, School of Chemistry, Cardiff University, Main Building, Park Place, Cardiff CF10 3AT, U.K.

* Supporting Information

ABSTRACT: Mesoporous silica-supported Ni-Zr catalysts prepared via the modified impregnation method by applying different solvents and calcination atmospheres were employed for CO methanation in a slurry-bed reactor. The results show that the glycerol-impregnated Ni-Zr/SiO_2 catalyst exhibited higher specific surface area and Ni species dispersion and more intensive nickel−support interaction than the water-impreg-nated one and thus enhanced the catalytic activity and stability. Furthermore, the carbon could be constructed on the surface of the Ni-Zr/SiO_2 catalyst from the carbonization of glycerol via calcination under an inert atmosphere and be removed through successive calcination in air. Owing to the improved nickel− support interaction, the carbon-sacrificed Ni-Zr/SiO_2 catalyst exhibited higher Ni dispersion and smaller and more uniform Ni particle sizes, leading to catalytic activity for CO methanation that is higher than that of the catalysts without carbonization.

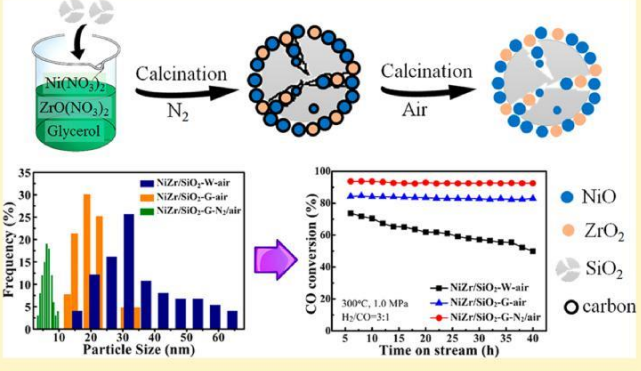

1. INTRODUCTION

Natural gas is a clean fossil fuel with high calorific value, and it is a good choice for meeting energy requirements in densely populated regions.[1−4] Because of the poor reserves and increasing demands for natural gas in China, it is effective to produce synthetic natural gas (SNG) from syngas, which can be obtained from the gasification of coal.[5−7] Moreover, the development of SNG could relieve the environmental pressure and improve the efficiency of energy-based processes. In the process of coal-to-SNG production, CO methanation is a key process during this transformation.[8,9] However, methanation is a highly exothermic reaction, and the high temperature may result in metal catalyst deactivation.[10−12] To solve this problem, industrial SNG production involves 2−4 fixed-bed methanation reactors to control the heat of reaction, resulting in high investment of equipment and complex technology.[13,14] A slurry reactor allows for isothermal temperature operation, which is suitable for the highly exothermic reactions,[15−17] such as Fischer−Tropsch synthesis.[15,18] Recently, slurry reactors have been intensively studied for methanation of CO or CO_2, because the CO equilibrium conversion of methanation is thermodynamically favored at low temperature, and the low and uniform reaction temperature could prevent catalyst sintering and carbon deposition.[19−22]

Ni/Al_2O_3 catalyst has been widely employed for the catalytic methanation reaction;[23,24] however, a nickel−aluminate spinel ($NiAl_2O_4$) was easily formed because of the strong interaction between NiO and Al_2O_3,[25,26] resulting in the decrease of the amount of active metallic Ni. Moreover, the Ni/Al_2O_3 catalyst suffered from rapid deactivation at high reaction temperature due to the metallic Ni sintering and carbon deposition.[23] On the other hand, the Ni/Al_2O_3 catalyst exhibited lower CO methanation activity at low reaction temperature, compared with the Ni/SiO_2 or Ni/ZrO_2 catalyst.[27] Among these supported catalysts, the Ni/ZrO_2 catalyst exhibited the best activity for CO methanation at low temperature.[28] However, our previous studies[29] showed that the Ni/ZrO_2 catalyst deactivated quickly in a slurry methanation reaction, resulting from the metallic Ni sintering. To improve the stability of the ZrO_2-supported Ni catalyst, a mixed oxide support is needed.[30,31]

There are many advantages to using mesoporous silica nanoparticles as a support, as it provides a mesoporous structure with tunable nanosize pores and high surface area.[32,33] The mesoporous SiO_2-supported Ni catalyst, without the formation of a $NiAl_2O_4$ spinel, are widely applied in many reactions.[9,34−36] However, the metallic Ni particles, highly dispersed in mesoporous silica channels, could still migrate from the pores to the external surface at high temperatures,

Table 1. Preparation Details of the NZ/SiO_2 Catalysts

sample	solvent	drying temperature (°C)	calcination temperature (°C)	calcination atmosphere and time
NZ/SiO_2-W-air	deionized water	120	500	in air for 4 h
NZ/SiO_2-G-air	60 wt % glycerol aqueous solution	240	500	in air for 4 h
NZ/SiO_2-G-N_2	60 wt % glycerol aqueous solution	240	500	in N_2 for 2 h
NZ/SiO_2-G-N_2/air	60 wt % glycerol aqueous solution	240	500	first in N_2 for 2 h, then in air for 2 h

owing to the weak interaction between the metallic particles and silica support; then, the sintering of metallic Ni particles is inevitable in these silica-supported catalysts. To solve this problem, studies have focused on encapsulation techniques or core−shell structures to confine the active metals.[37,38] Though it is an effective way to stabilize the active metals on the SiO_2 supports,[39,40] the encapsulated or core−shell catalysts do not work well in a three-phase slurry-bed reactor, especially when a high-viscosity liquid (such as liquid paraffin) is selected as the inert medium. This is because high-viscosity liquids increase the mass-transfer resistance and decrease the frequency of molecular collisions,[41] resulting in poor catalytic activity.

Recently, the isolation effects of carbon templates were studied to prevent the growth of metal nanoparticles on a series of supports, thus controlling the particle size and improving the metal dispersion. Cheng et al.[42] precoated the amorphous silica with glucose aqueous solutions to prepare a carbon-encapsulated cobalt catalyst, which exhibited a smaller nano-particle size of cobalt oxide and a higher catalytic performance for Fischer−Tropsch synthesis. Zhan et al.[43] found that sacrificial carbon layers could be constructed on the surface of supported Au catalysts using dopamine, which could lead to good coking and sintering resistance and thus enhanced stability of Au catalyst. However, few studies on sacrificing carbon strategy for silica-supported Ni catalyst have been reported, especially when the Ni catalyst was employed for CO methanation in a three-phase slurry-bed reactor.

Our previous studies[29,44] showed that the Ni-Zr catalyst exhibited high activity for CO methanation in a slurry-bed reactor. Herein, to continue the research work on enhancement of catalytic activity as well as the stability of Ni-Zr/SiO_2 catalysts for slurry methanation, mesoporous silica-supported Ni-Zr catalysts were prepared by the modified impregnation method. The carbon was constructed on the surface of Ni-Zr/ SiO_2 catalyst and then sacrificed by annealing in air to obtain highly dispersed Ni nanoparticles. Also, a Ni-Zr/SiO_2 catalyst without carbon was used as a reference. The effect of carbon on the physiochemical properties and catalytic performance was discussed. The catalysts were characterized by means of X-ray diffraction (XRD), thermogravimetric mass spectrometry (TG-MS), N_2 adsorption−desorption, H_2 temperature-programmed reduction (H_2-TPR), H_2-chemisorption, CO temperature-programmed desorption (CO-TPD), X-ray photoelectron spectroscopy (XPS), and transmission electron microscopy (TEM) to clarify the influence of Ni dispersion, Ni particle size, and metal−support interaction on methanation performance. It is illustrated that mesoporous silica-supported Ni-Zr catalysts, prepared by a sacrificial carbon method, lead to the enhancement in terms of catalyst activity and stability.

2. EXPERIMENTAL SECTION

2.1. Catalyst Preparation. Nickel(II) nitrate hexahydrate 99% was supplied by Sinopharm Chemical Reagent Co. Ltd., China. Zirconyl nitrate dihydrate 99.9% and glycerol 99% were purchased from Tianjin Guangfu Fine Chemical Research Institute, China. SiO_2 (0.2−0.3 μm, 195 m^2/g) was purchased from Sigma-Aldrich. Liquid paraffin was purchased from Tianjin Kemiou Chemical Reagent Co., Ltd., China. The feed gases (Taiyuan Iron & Steel (Group) Co., Ltd., China) were used as received.

Mesoporous silica-supported Ni-Zr catalysts were prepared by the glycerol modified impregnation method. The Ni metal loading on SiO_2 support was fixed at 20 wt %; Zr represents ZrO_2, and the loading was 5 wt %. To reduce the impact of viscosity on the solvent for catalyst preparation, 60 wt % glycerol balanced with deionized water was selected as solvent. Initially, 3.96 g of $Ni(NO_3)_2{\cdot}6H_2O$ and 0.50 g of $ZrO(NO_3)_2{\cdot}\ 2H_2O$ were dissolved in a 60 wt % glycerol aqueous solution; then 4.0 g of SiO_2 support was added slowly, and the mixture was stirred vigorously. The mixture was then treated ultrasoni-cally at 60 °C for 2 h to make the solution uniformly dispersed, followed by agitating and evaporating at 60 °C to obtain the solid. Finally, the solid was dried at 240 °C for 12 h and calcined successively at 500 °C in N_2 for 2 h before being calcined in air for another 2 h. The obtained Ni-Zr/SiO_2 catalyst was denoted as NZ/SiO_2-G-N_2/air, where G represents glycerol.

For comparison, a NZ/SiO_2-G-N_2 catalyst was prepared by applying glycerol aqueous solution as solvent and calcination in N_2 for 2 h (without calcination in air). A NZ/SiO_2-G-air catalyst was prepared from calcination in air for 4 h (without calcination in N_2). A NZ/SiO_2-W-air catalyst was also prepared by using deionized water as solvent and being calcined in air for 4 h. The details are summarized in Table 1.

2.2. Catalyst Characterization. Thermogravimetric mass spectrometry was performed using a Perkin-Elmer (Pyris One) TGA coupled with a Clarus SQ 8 mass spectrometer. The sample was heated in a flow of air (80 mL/min) from room temperature to 900 °C at a heating rate of 10 °C/min.

Inductively coupled plasma atomic emission spectrometry (ICP-AES) measurement was carried out on an IRIS Intrepid II XSP instrument to do elemental analysis of the catalyst.

Powder X-ray diffraction (XRD) was performed using a PANalytical X'pert Pro diffractometer employing a Cu Kα (λ = 0.154 056 nm) radiation source operating at 40 kV and 40 mA. The scanning speed was 4 °/min in 2θ range from 10° to 80° using a step size of 0.016°. An in situ Anton Paar XRK900 cell was used to monitor the changes of the phase during the reduction process, here, a flow of 5% H_2/95% Ar (30 mL/min) was passed through the sample bed while the cell was heated from 30 to 550 °C, at a ramp rate of 20 °C/min. The sample was then cooled to room temperature before the diffraction pattern over the same 2θ range was recorded.

The N_2 adsorption−desorption isotherms were obtained using a Beishide 3H-2000PS2 at −196 °C. Prior to the tests, the samples were degassed at 250 °C for 3 h in a high vacuum. The specific surface areas were calculated by the Brunauer−Emmett−Teller (BET) method, while the average pore diameters and pore volumes were obtained by the Barrett−

Joyner−Halenda (BJH) method from the desorption branches of the N_2 isotherms.

H_2 temperature-programmed reduction was carried out on a Micrometrics Autochem II 2920 instrument. Before the measurements, 20 mg of each calcined catalyst was first pretreated at 350 °C, at 10 °C/min for 30 min, in flowing He (50 mL/min) to remove moisture and impurities. After the sample was cooled to room temperature, a 10% H_2/90% Ar (50 mL/min) gas mixture was introduced, and subsequently the sample was heated to 800 °C at a ramp rate of 10 °C/min. For H_2 chemisorption analysis, 200 mg of the sample was reduced at 550 °C for 2 h under 10% H_2/Ar flow (30 mL/min). After the sample cooled to 40 °C, the chemisorption was carried out by pulsing a mixture of 10% H_2/Ar (30 mL/min). The Ni dispersion was calculated by assuming the stoichiometric ratio of $H_{adsorbed}/Ni_{surface}$ equals 1.[45] For CO-TPD analysis, 200 mg of each sample was first pretreated at 350 °C for 30 min in a He stream (30 mL/min) and then cooled to 50 °C. A stream of pure CO (99.99%, 50 mL/min) gas was introduced for 1 h and then purged with a He stream for 1 h to remove the excessive CO. Finally, samples were heated to 600 °C under a He flow at 10 °C/min.

X-ray photoelectron spectroscopy analysis was obtained using a Thermo Scientific K-Alpha$^+$ spectrometer using monochromatic Al Kα radiation (hν = 1486.6 eV), and charge neutralization was performed using a combination of low-energy electrons and argon ions, resulting in a C(1s) energy of 284.8 eV for the adventitious carbon peak.

Sample morphology and particle size were observed by TEM using a JEOL JEM-2100F microscope operating at 200 kV. Prior to the tests, well-ground powdered samples were dispersed in ethanol using ultrasonic treatment for 10 min before the suspension was dripped onto a copper grid for analysis.

2.3. Catalytic Performance Evaluation. The activity test of NZ/SiO_2 catalysts for CO methanation was performed using a 250 mL slurry-bed reactor. Prior to testing, each calcined catalyst (100−140 mesh) was reduced at 500 °C for 4 h in a flowing of 25% H_2/75% N_2 gas mixture. Then, 1.0 g of reduced catalyst and 120 mL of liquid paraffin were mixed in a slurry-bed reactor with a rotating speed of 750 r/min; after that, pure nitrogen was introduced to remove the air, followed by increasing the temperature to 300 °C and pressure to 1.0 MPa. The pure N_2 was then switched to the reactant gas (75% H_2/ 25% CO) with a space velocity of 6000 $mL \cdot g^{-1} \cdot h^{-1}$. The outlet gas was cooled to 2 °C and quantitatively analyzed by online gas chromatography (Agilent 7890A), equipped with three valves and four columns, using a thermal conductivity detector (TCD) and a flame ionization detector (FID). The details of analysis and calculation of conversion of CO and selectivity of CH_4, CO_2, and C_i (i = 2, 3, and 4) were shown in our previous studies.[13,16]

3. RESULTS AND DISCUSSION

3.1. TG-MS and ICP-AES Analysis. The TG-MS technique was used to study the weight loss of the calcined catalysts and determine the components of an evolved gas from the TG analysis. The curves of the catalysts are presented in Figure 1a. It could be found from the TG curves that when the temperature was higher than 300 °C, the NZ/SiO_2-G-N_2/air catalyst showed a slightly higher weight loss than the NZ/SiO_2-W-air catalyst. The NZ/SiO_2-G-N_2 catalyst, calcined in N_2 atmosphere, showed a slight increase in mass in the temperature range of 200−300 °C and a significant decrease in the range of 300−900 °C. The increase in mass was due to the oxidation of Ni metal to NiO in air, while the decrease at high temperature resulted from the oxidation of carbon in air. It is clear that a redox reaction occurred during the catalyst calcination process, and the metal nitrate acted as an oxidizing agent while the glycerol acted as a reducing agent;[46] overall, this made the $Ni(NO_3)_2$ reduce to Ni metal. Figure 1a also shows that the NZ/SiO_2-G-N_2 catalyst exhibited the detection of significant CO_2 formation by the MS signal (m/e = 44) during the calcination in air, compared with NZ/SiO_2-G-N_2/air catalyst. To further confirm the existence of carbon, these catalysts were dissolved in aqua regia using a 25 mL volumetric flask at room temperature overnight, with a photograph shown in Figure 1b. It was found that the NZ/SiO_2-W-air and NZ/ SiO_2-G-N_2/air catalysts completely dissolved in aqua regia while the NZ/SiO_2-G-N_2 catalyst showed a black undissolved substance, confirming the existence of carbon.

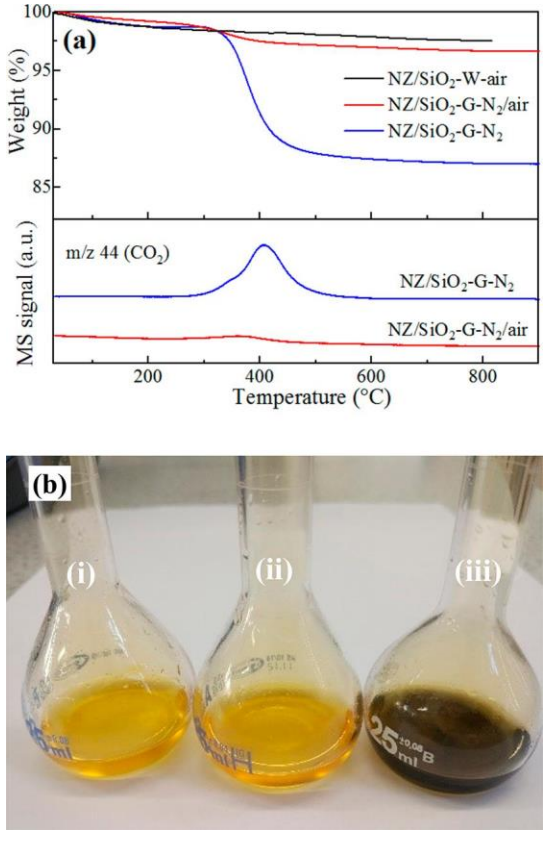

Figure 1. TG-MS curves (a) and a photograph (b) of the calcined NZ/SiO_2 catalysts: (i) NZ/SiO_2-W-air, (ii) NZ/SiO_2-G-N_2/air, and (iii) NZ/SiO_2-G-N_2

The real Ni and Zr loadings of the calcined NZ/SiO_2 catalysts are obtained from ICP-AES results as listed in Table 2. It is clear that the real Ni and Zr loadings were slightly lower than the designed values. However, the Ni loading of each catalyst was very close, indicating that the nickel was successfully loaded on the SiO_2 support as planned.

3.2. XRD Analysis. The calcined NZ/SiO_2 catalysts were characterized by powder XRD with their patterns shown in Figure 2a. The broad peaks around 22° were attributed to amorphous silica, while the diffraction peaks at 2θ angles of 37.3°, 43.3°, 62.9°, 75.4°, and 79.4° were recognized as cubic NiO (JCPDS No. 47-1049). NZ/SiO_2-W-air catalyst, prepared

Table 2. Detailed Physicochemical Properties of Bare SiO_2 Support and Calcined NZ/SiO_2 Catalysts

sample	specific surface area ($m^2 \cdot g^{-1}$)[a]	pore volume ($cm^3 \cdot g^{-1}$)[b]	average pore diameter (nm)[c]	loading (wt %)[d]	
				Ni	Zr
SiO_2	196	1.53	27.2	–	–
NZ/SiO_2-W-air	159	0.96	16.0	18.18	3.33
NZ/SiO_2-G-air	193	1.18	14.8	18.28	3.29
NZ/SiO_2-G-N_2	226	1.03	14.2	–	–
NZ/SiO_2-G-N_2/air	203	1.08	16.5	18.39	3.29

[a]Calculated by the BET equation. [b]BJH desorption pore volume. [c]BJH desorption average pore diameter. [d]Determined by ICP-AES measurement.

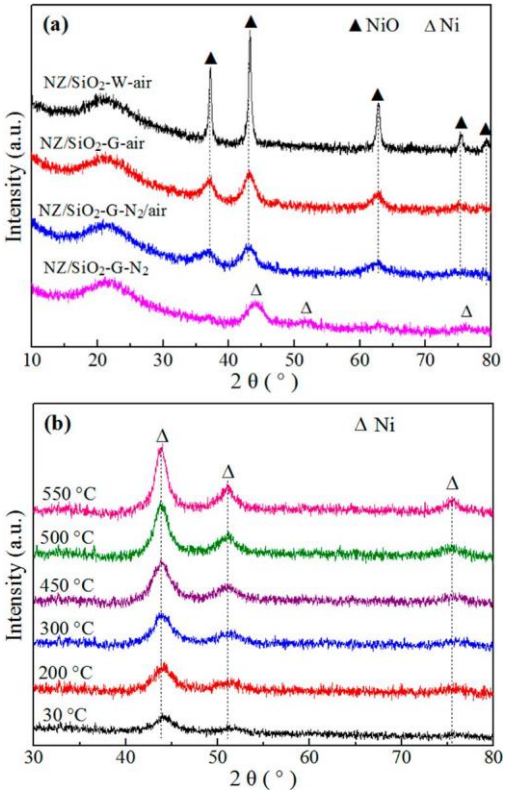

Figure 2. Powder XRD patterns of the calcined NZ/SiO_2 catalysts (a) and in situ XRD patterns of NZ/SiO_2-G-N_2 catalyst during the reduction process (b).

by using water as solvent, exhibited the strongest peak intensity for NiO. By using glycerol as solvent, the peak intensity for NZ/SiO_2-G-air and NZ/SiO_2-G-N_2/air catalysts significantly decreased. Moreover, the half width for NiO peaks of both catalysts at 37.3° and 43.3° became broader. These results suggest that the dispersion of NiO remarkably improved. The NZ/SiO_2-G-N_2 catalyst with the produced carbon from carbonization of glycerol exhibited no diffraction peaks of graphite, indicating the existence of amorphous carbon, combined with TG-MS results. No significant diffraction peaks attributed to NiO were observed. Instead, the obvious diffraction peaks at 2θ of 44.5°, 51.8°, and 76.4° appeared, attributed to metallic Ni (JCPDS No. 65-2865). In addition, no significant diffraction peaks attributed to ZrO_2 were observed, indicating that the ZrO_2 was amorphous or the amount of ZrO_2 was below the detection limit of XRD.

The in situ XRD patterns of NZ/SiO_2-G-N_2 catalyst during the reduction process in a H_2 atmosphere are shown in Figure 2b. All the diffraction peaks were attributed to metallic Ni, and no peaks corresponding to NiO species were detected. For comparison, the in situ XRD patterns of NZ/SiO_2-G-air and NZ/SiO_2-G-N_2/air catalysts during the reduction process are shown in Figure S1 (see the Supporting Information). It could be found that the NiO species of both catalysts were reduced to metallic Ni when the reduction temperature reached 500 °C or above, suggesting that 500 °C was enough for the catalyst reduction.

3.3. Textural Properties. N_2 adsorption−desorption was performed to investigate the porosity of bare SiO_2 support and calcined catalysts. The SiO_2 support and all catalysts exhibited a type IV adsorption isotherm characteristic of mesoporous materials (see Figure S2). The specific surface areas of SiO_2 support and calcined catalysts were measured by the BET method, and the results are summarized in Table 2. SiO_2 support possessed the specific surface area of 196 m^2/g, the highest pore volume of 1.53 $cm^3 \cdot g^{-1}$, and the average pore diameter of 27.2 nm. NZ/SiO_2-W-air catalyst exhibited the lowest specific surface area of 159 m^2/g and pore volume of 0.96 $cm^3 \cdot g^{-1}$ because of the blockage of nickel oxide and zirconia in pores. After the introduction of glycerol, NZ/SiO_2 catalysts showed an apparent increase in specific surface area and pore volume. This is attributed to glycerol that improved the dispersion of nickel oxide and zirconia, which decreased the blockage of pores. Interestingly, the precarbonized NZ/SiO_2-G-N_2 catalyst exhibited the highest specific surface area and the lowest average pore diameter, accounting for the produced amorphous carbon, as confirmed from TG-MS and XRD results, which increased the specific surface area. Further calcined in air, the NZ/SiO_2-G-N_2/air catalyst showed a slight decrease in specific surface area and increase in pore volume and average pore diameter, which were due to the sacrifice of produced carbon in the calcination process.

3.4. H_2-TPR Analysis. The reduction behavior of the Ni species, including the interaction between metal and support, can be evaluated using the TPR technique. Figure 3 displays the H_2-TPR profiles of the NZ/SiO_2 catalysts. The reducibility of NiO on the support depends on the nickel−support interaction, and the more intense interaction leads to more difficulty for NiO reduction.[47] All the catalysts showed different reduction peaks, which were related to the reduction of NiO. The overlapping peaks can be deconvoluted by using Gaussian-type functions, and these reducible NiO species could be divided into three types: α, β, and γ.[23] Quantitative analysis results for these types of NiO species of the TPR profiles are shown in Table 3. The α-NiO in the low-temperature region was assigned to the reduction of bulk NiO, which either weakly interacted with the support or had no contact at all with it. This type of NiO species can easily migrate and grow into large particles at high temperature. The β-NiO at medium temper-ature had moderate interactions with the support, while the γ-NiO represented the strongest interactions between the NiO species and support. It is believed that the β- and γ-NiO at

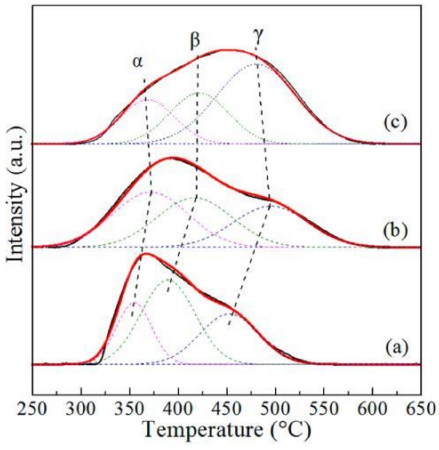

Figure 3. H_2-TPR profiles of calcined NZ/SiO_2 catalysts: (a) NZ/SiO_2-W-air, (b) NZ/SiO_2-G-air, and (c) NZ/SiO_2-G-N_2/air.

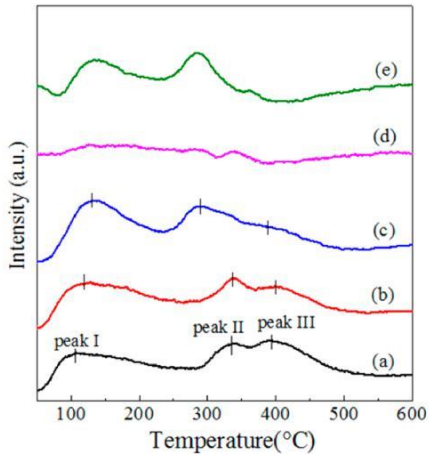

Figure 4. CO-TPD profiles of NZ/SiO_2 catalysts: (a) NZ/SiO_2-W-air, (b) NZ/SiO_2-G-air, (c) NZ/SiO_2-G-N_2/air, (d) subtracting curve a from curve b, and (e) subtracting curve a from curve c.

higher temperatures resulted from a fine dispersion of the NiO precursor and smaller NiO particles.[16,48]

As shown in Figure 3 and Table 3, the deconvoluted reduction peaks of β- and γ-NiO for NZ/SiO_2-G-air and NZ/SiO_2-G-N_2/air significantly shifted to higher temperatures, compared with those of NZ/SiO_2-W-air, indicating that the glycerol as solvent strengthens the interaction between nickel and support. Moreover, the NZ/SiO_2-G-N_2/air catalyst exhibited the largest reduction peak of γ-NiO, which indicated that the carbonization of glycerol enhanced the nickel−support interaction. The strong interaction between nickel and the support could effectively inhibit the sintering of Ni particles and thus lead to the formation of small Ni particles, which is beneficial to good catalytic stability of the catalyst.

3.5. H_2 Chemisportion and CO-TPD Analysis. The H_2 chemisorption technique was used to determine the active Ni dispersion and average size of the Ni particles, assuming a stoichiometric factor of $H_{adsorbed}/Ni_{surface}$ = 1.[45] The results are summarized in Table 3. NZ/SiO_2-W-air catalyst exhibited the lowest metallic Ni dispersion (3.3%) and largest Ni particles size (30.7 nm). After glycerol was introduced, the NZ/SiO_2-G-air and NZ/SiO_2-G-N_2/air catalysts showed a significant increase in Ni dispersion and decrease in Ni particle size. This was more apparent for NZ/SiO_2-G-N_2/air catalyst where the Ni dispersion increased to 7.1% and the Ni particles size decreased to 14.2 nm.

CO-TPD analysis was carried out to investigate the adsorption type and strength of the CO species on NZ/SiO_2 catalysts, with the results shown in Figure 4. Multiple CO desorption peaks were found between 50 and 250 °C and between 250 and 500 °C. The different desorption peaks indicate the presence of various types of adsorbed CO species.[6,49] The low-temperature desorption peaks (peak I) resulted from the desorption of weakly adsorbed CO on catalyst surface, which contributed little toward methanation.[50] The high-temperature desorption peaks (peaks II and III) represented the desorption of strongly adsorbed CO species, which took part in activating CO molecules in methanation reaction.[51] As shown in Figure 4, the desorption temperature of peak I of NZ/SiO_2-G-N_2/air catalyst shifted to higher temperature, while the temperature of peak II shifted to lower temperature, compared with NZ/SiO_2-W-air catalyst. Moreover, the peak area of III of the NZ/SiO_2-G-N_2/air catalyst significantly decreased, indicating that the dispersion of active sites for CO adsorption was more uniform. For comparison, curve d was obtained through subtracting curve a from curve b, while curve e was obtained from subtracting curve a from curve c.[52] It can be seen that curve e exhibited two main desorption peaks, while curve d showed very weak desorption peaks. In addition, the amounts of CO desorption listed in Table 3 showed that NZ/SiO_2-G-N_2/air possessed the largest amount of desorbed CO (0.58 mmol/g_{cat}). The results indicated that NZ/SiO_2-G-N_2/air catalyst had a higher amount of active CO molecules, which was beneficial to the methanation reaction.

3.6. XPS Analysis. XPS analysis was performed to determine the oxidation states and elemental molar atomic ratios of surface species of calcined catalysts. The spectra of Ni $2p_{3/2}$ are displayed in Figure 5; the binding energies (BEs) and the surface atomic Ni/Zr and C/Ni ratio are summarized in Table 4. The NZ/SiO_2-G-N_2 catalyst exhibited the BEs of Ni $2p_{3/2}$ at 852.1 eV that can be associated to Ni metal on the catalyst surface, indicating the formation of metallic Ni after calcination in N_2. The peak located at 855.2 eV was associated to Ni $2p_{3/2}$ of Ni^{2+}, which perhaps arose from the reoxidation of

Table 3. Gaussian Fitting Analysis of TPR Profiles, H_2-Chemisorption, and CO Desorption Results of NZ/SiO_2 Catalysts

	reduction temperature (°C)			relative content (%)					
sample	α	β	γ	α	β	γ	Ni dispersion (%)[a]	Ni particle size (nm)[a]	amount of CO desorption (mmol/g)
NZ/SiO_2-W-air	355.3	390.0	453.0	22.4	46.9	30.7	3.3	30.7	0.51
NZ/SiO_2-G-air	372.3	417.3	495.7	37.8	33.9	28.3	4.9	20.5	0.43
NZ/SiO_2-G-N_2/air	369.8	422.4	480.9	20.4	25.8	53.8	7.1	14.2	0.58

[a]Determined by H_2 chemisorption, assuming the stoichiometry of $H_{adsorbed}/Ni_{surface}$ = 1

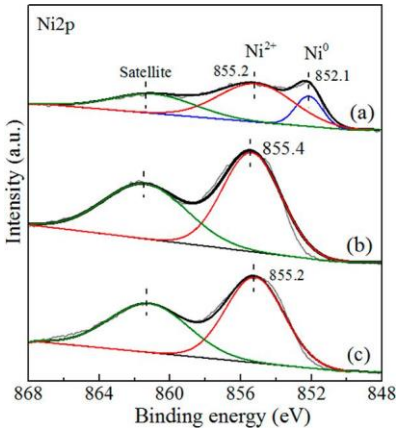

Figure 5. Ni 2p XPS profiles of the calcined NZ/SiO_2 catalysts: (a) NZ/SiO_2-G-N_2, (b) NZ/SiO_2-G-N_2/air, and (c) NZ/SiO_2-G-air.

Table 4. Binding Energy of Ni $2p_{3/2}$ and Atomic Ratio of the Calcined NZ/SiO_2 Catalysts

	Ni $2p_{3/2}$ binding energy (eV)		atomic ratio	
sample	Ni^{2+}	Ni^0	Ni/Zr	C/Ni
NZ/SiO_2-G-N_2	855.2	852.1	5.8	8.91
NZ/SiO_2-G-N_2/air	855.4	–	6.2	1.09
NZ/SiO_2-G-air	855.2	–	5.4	1.08

Ni metal in air before the XPS experiments.[13] After calcination in air, the peak for Ni metal of NZ/SiO_2-G-N_2/air and NZ/ SiO_2-G-air catalysts disappeared, while the peak intensity of both catalysts significantly increased, compared with NZ/SiO_2-G-N_2, suggesting the carbon covered the surface of the NZ/SiO_2-G-N_2 catalyst. In Table 4, it is interesting to find that the NZ/SiO_2-G-N_2/air catalyst exhibited BEs (855.4 eV) that are slightly higher than that of the NZ/SiO_2-G-air catalyst (855.2 eV), and the BEs of both catalysts are higher than that of pure NiO (854.4 eV).[13] The results indicated that the nickel−support interaction of the NZ/SiO_2-G-N_2/air catalyst is stronger than that of the NZ/SiO_2-G-air catalyst, consistent with the TPR results. The atomic Ni/Zr ratio of the NZ/SiO_2-G-air catalyst, as shown in Table 4, was only 5.4, which was lower than that of NZ/SiO_2-G-N_2 and NZ/SiO_2-G-N_2/air catalysts, indicating more Ni atoms are exposed on the surface of the NZ/SiO_2-G-N_2/air catalyst. Moreover, the NZ/SiO_2-G-N_2 catalyst showed a C/Ni ratio (8.91) much higher than that of the catalysts calcined in air, which was due to the carbonization of glycerol on the surface of the NZ/SiO_2-G-N_2 catalyst calcined in N_2 atmosphere.

3.7. TEM Analysis. TEM and HRTEM images of the calcined catalysts are shown in Figure 6 and Figure S3, respectively. In these images, the light gray and black particles represent the silica particles and NiO particles, respectively. Figure 6a shows that the NZ/SiO_2-W-air catalyst exhibited an agglomeration of NiO particles, with the average NiO particles size centered at ~32 nm, as shown in Figure 6d. After glycerol is introduced, the NZ/SiO_2-G-air catalyst (Figure 6b) showed a high dispersion of NiO particles with the size centered at ~19 nm, indicating that the glycerol played an important role in enhancing the NiO dispersion. Figure 6c shows that the NZ/SiO_2-G-N_2/air catalyst, first calcined in N_2 and then in air, exhibited the most uniform and highly dispersed NiO particles, with an average size centered at ~7 nm. Moreover, the particle sizes of NiO for all the catalysts could also be identified by HRTEM from Figure S3, as well as the lattice fringes of NiO. The results show that the NZ/SiO_2-G-N_2/air catalyst

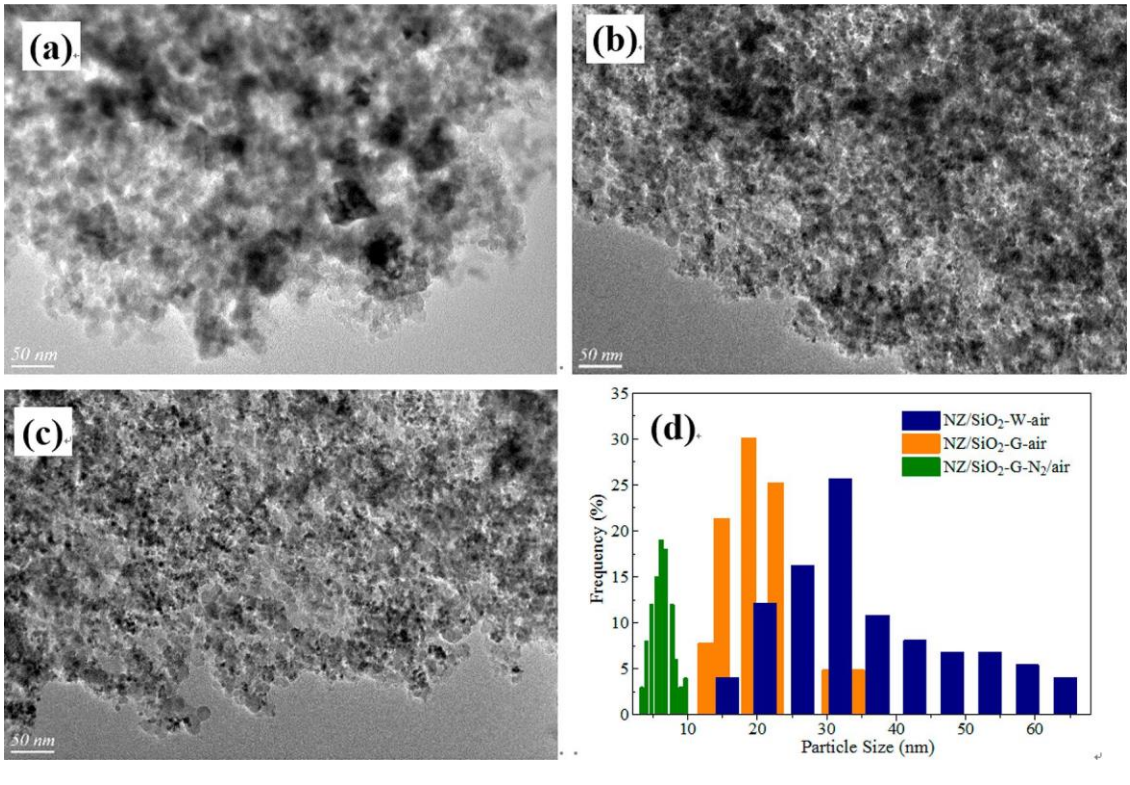

Figure 6. TEM images of the calcined NZ/SiO_2 catalysts: (a) NZ/SiO_2-W-air, (b) NZ/SiO_2-G-air, (c) NZ/SiO_2-G-N_2/air, and (d) the NiO particle size distributions

carbonized by glycerol prevents the agglomeration of NiO particles and formed smaller NiO particles.

3.8. Catalyst Performance for Three-Phase CO Methanation. The catalytic performance of NZ/SiO_2 catalysts for CO methanation was investigated at 300 °C and 1.0 MPa in a slurry-bed reactor. The CO conversion with a reaction of 40 h is shown in Figure 7a. NZ/SiO_2-W-air catalyst exhibited a fast deactivation from 73% to 43% in terms of CO conversion, while the NZ/SiO_2-G-air catalyst, prepared with glycerol as solvent and calcined in air, exhibited a high and stable catalytic activity of 83%. The NZ/SiO_2-G-N_2/air catalyst, which sacrificed the carbon from the carbonization of glycerol, exhibited the highest activity for the CO conversion of 93%, and no deactivation was observed. During the reaction process, all the catalysts exhibited stable selectivity for CH_4, CO_2, and C_{2-4}, with the average selectivity data of each catalyst shown in Figure 7b. The NZ/SiO_2-W-air catalyst showed a selectivity of 90.8% for CH_4, 1.8% for C_{2-4} hydrocarbons, and 7.4% for CO_2. In comparison, the NZ/SiO_2-G-N_2/air catalyst exhibited a slightly higher CH_4 selectivity (91.4%) and lower CO_2 selectivity (6.0%). The CO_2 selectivity decreased in the order of NZ/SiO_2-W-air, NZ/SiO_2-G-air, and NZ/SiO_2-G-N_2/air, which also correlates with a decrease in Ni particles size. Both NZ/SiO_2-G-air and NZ/SiO_2-G-N_2/air catalysts exhibited high stability at low temperatures, and their average activity and selectivity at each temperature for 20 h are shown in Figure S4. Compared with the NZ/SiO_2-G-air catalyst, the NZ/SiO_2-G-N_2/air catalyst showed higher CO conversion and CH_4 and CO_2 selectivity and lower C_{2-4} selectivity.

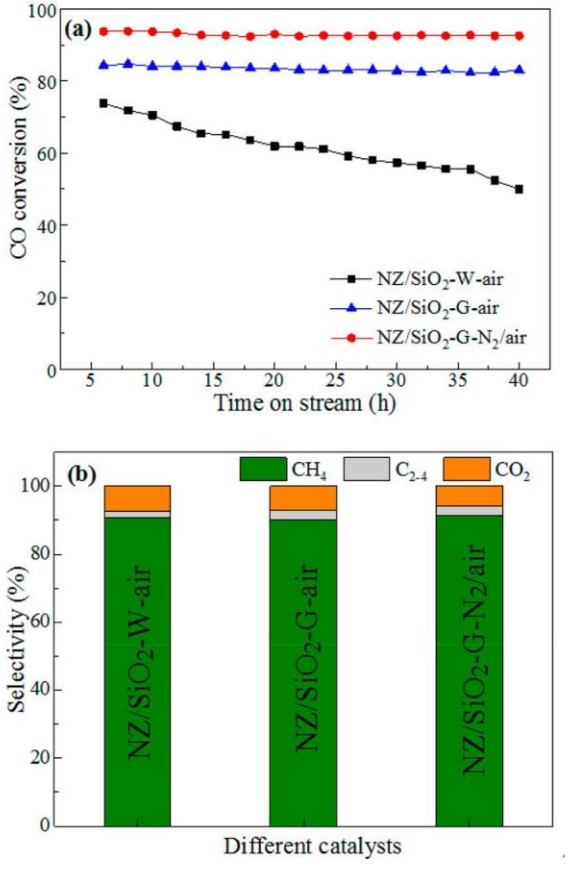

Figure 7. Catalytic performance for CO methanation over NZ/SiO_2 catalysts: (a) CO conversion and (b) selectivities for CH_4, C_{2-4}, and CO_2.

3.9. Discussion. The impregnation method has been widely applied in catalyst preparation because of its simple and fast operation.[53,54] However, the choice of preparation conditions, such as metal precursor, impregnation solvent, calcination temperature, time, and atmosphere, could all affect the catalyst physiochemical properties and thus change the catalytic performance.[13,49,55] In this study, NZ/SiO_2 catalyst was prepared by the modified impregnation method. The glycerol-impregnated sample was first calcined in an inert atmosphere in order to carbonize the glycerol on the surface of the support. It was found that when calcined in the N_2 atmosphere, the precursor of nickel nitrate converted to Ni metal without the formation of NiO, and the excess glycerol formed carbon. When calcined in air, the nickel nitrate converted to nickel oxide, and the excess glycerol converted to CO_2 and water. Powder XRD analysis confirmed the existence of Ni metal and nickel oxide for the catalyst calcined in N_2 and air, respectively. Moreover, TG-MS results and photographs confirmed the presence of carbon.

Compared with the NZ/SiO_2-W-air catalyst, prepared by applying water as solvent, NZ/SiO_2 catalysts using glycerol as solvent exhibited an improved dispersion of NiO, as shown in Figure 2a. The results in Table 3 and Figure 6 illustrate that different calcination atmospheres resulted in different particle size of Ni species. The effect of calcination atmosphere on the dispersion and particles size of Ni species is displayed in Scheme 1. The NZ/SiO_2-G-air catalyst calcined in air has undergone the redox reaction, and the excess glycerol converted to CO_2 and water.[46] For the NZ/SiO_2-G-N_2 catalyst calcined in a N_2 atmosphere, a redox reaction also occurred; moreover, the carbon was produced on the surface of the support from the carbonization of excess glycerol. The

Scheme 1. Effect of Calcination Atmosphere on Ni Species' Dispersion and Particle Size

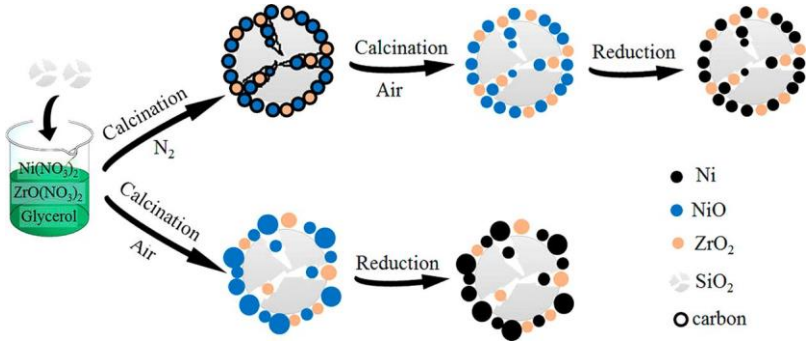

produced carbon on the catalyst surface enhanced the interaction between Ni species and support, and thus inhibited the migration of Ni species during the calcination and reduction process, and formed small Ni particles size, as confirmed by TEM and TPR analysis. Furthermore, the H_2-chemisorption and CO-TPD results in Table 3 showed that the produced carbon on the catalyst surface was beneficial to the formation of smaller Ni particles, higher metal surface area, and a greater amount of active sites. The abovementioned physiochemical properties led to the enhancement of catalyst activity and stability for CO methanation, as shown in Figure 6, while larger Ni particle sizes resulted in inferior activity and stability.

4. CONCLUSIONS

Ni-Zr catalysts supported on mesoporous SiO_2 have been synthesized via the modified impregnation method and applied for CO methanation in a slurry-bed reactor. The effect of solvent and carbonization was discussed. The glycerol-impregnated NZ/SiO_2 catalyst exhibited much lower NiO diffraction peaks than the water-impregnated catalyst, indicating the higher Ni species dispersion and smaller Ni particle size. Moreover, the glycerol-impregnated catalyst exhibited higher specific surface area and more intensive nickel−support interaction and thus enhanced the catalytic activity and stability. Furthermore, the carbon was constructed on the surface of NZ/SiO_2 catalyst from the carbonization of glycerol via calcination under an inert atmosphere and was removed through the successive calcination in air. The carbonized NZ/ SiO_2 catalyst exhibited the diffraction peaks of metallic Ni and almost no diffraction peaks of NiO. Owing to the improved nickel−support interaction, the carbon-sacrificed NZ/SiO_2 catalyst owned higher Ni dispersion and smaller and uniform Ni particle sizes, leading to higher catalytic activity for CO methanation than the catalysts without carbonization. In short, the carbon-sacrificed strategy is very effective for preparing the supported metal catalyst with high metal dispersion and small metal particles.

ASSOCIATED CONTENT

* Supporting Information

In-situ XRD patterns of NZ/SiO_2-G-air and NZ/SiO_2-G-N_2/air catalysts during the reduction process in a H_2 atmosphere, N_2 adsorption−desorption isotherms and pore size distribution curves of bare SiO_2 support and calcined catalysts, HRTEM images of the calcined NZ/SiO_2 catalysts, and effect of sacrificed carbon on methanation performance over NZ/SiO_2-G catalyst prepared by using glycerol as solvent (PDF)

AUTHOR INFORMATION

Corresponding Authors

*No. 79 Yingze West street, Taiyuan 030024, Shanxi, China. E-mail: mengfanhui@tyut.edu.cn. Tel./fax: +86-351-6018526.

*No. 79 Yingze West street, Taiyuan 030024, Shanxi, China. E-mail: lizhong@tyut.edu.cn. Tel./fax: +86-351-6018526.

ORCID

Fanhui Meng: 0000-0003-0998-5179

David J. Morgan: 0000-0002-6571-5731

Zhong Li: 0000-0001-6087-6854

Notes

The authors declare no competing financial interest.

ACKNOWLEDGMENTS

This work was supported by the Youth Foundation of Shanxi Province (No. 2013021007-4). The first author's academic scholarship to Cardiff University has been financially supported by China Scholarship Council (No. 201606935030).

REFERENCES

(1) Liu, J.; Wang, E.; Lv, J.; Li, Z.; Wang, B.; Ma, X.; Qin, S.; Sun, Q. Investigation of Sulfur-resistant, Highly Active Unsupported MoS_2 Catalysts for Synthetic Natural Gas Production from CO Methanation. Fuel Process. Technol. 2013, 110, 249.

(2) Li, S.; Ji, X.; Zhang, X.; Gao, L.; Jin, H. Coal to SNG: Technical Progress, Modeling and System Optimization through Exergy Analysis. Appl. Energy 2014, 136, 98.

(3) Zhao, K.; Wang, W.; Li, Z. Highly Efficient Ni/ZrO_2 Catalysts Prepared via Combustion Method for CO_2 Methanation. J. CO_2 Util. 2016, 16, 236.

(4) Ren, J.; Li, H.; Jin, Y.; Zhu, J.; Liu, S.; Lin, J.; Li, Z. Silica/titania Composite-supported Ni Catalysts for CO Methanation: Effects of Ti Species on the Activity, Anti-sintering, and Anti-coking Properties. Appl. Catal., B 2017, 201, 561.

(5) Tao, M.; Xin, Z.; Meng, X.; Bian, Z.; Lv, Y. Highly Dispersed Nickel within Mesochannels of SBA-15 for CO Methanation with Enhanced Activity and Excellent Thermostability. Fuel 2017, 188, 267.

(6) Razzaq, R.; Li, C.; Usman, M.; Suzuki, K.; Zhang, S. A Highly Active and Stable Co_4N/γ-Al_2O_3 Catalyst for CO and CO_2 Methanation to Produce Synthetic Natural Gas (SNG). Chem. Eng. J. 2015, 262, 1090.

(7) Liu, Q.; Qiao, Y.; Tian, Y.; Gu, F.; Zhong, Z.; Su, F. Ordered Mesoporous Ni−Fe−Al Catalysts for CO Methanation with Enhanced Activity and Resistance to Deactivation. Ind. Eng. Chem. Res. 2017, 56, 9809.

(8) Shinde, V. M.; Madras, G. CO Methanation toward the Production of Synthetic Natural Gas over Highly Active Ni/TiO_2 Catalyst. AIChE J. 2014, 60, 1027.

(9) Gao, J.; Liu, Q.; Gu, F.; Liu, B.; Zhong, Z.; Su, F. Recent Advances in Methanation Catalysts for the Production of Synthetic Natural Gas. RSC Adv. 2015, 5, 22759.

(10) Bian, L.; Wang, W.; Xia, R.; Li, Z. Ni-based Catalyst Derived from Ni/Al Hydrotalcite-like Compounds by the Urea Hydrolysis Method for CO Methanation. RSC Adv. 2016, 6, 677.

(11) Yu, Y.; Jin, G.-Q.; Wang, Y.-Y.; Guo, X.-Y. Synthetic Natural Gas from CO Hydrogenation over Silicon Carbide Supported Nickel Catalysts. Fuel Process. Technol. 2011, 92, 2293.

(12) Rönsch, S.; Schneider, J.; Matthischke, S.; Schlüter, M.; Götz, M.; Lefebvre, J.; Prabhakaran, P.; Bajohr, S. Review on Methanation − from Fundamentals to Current Projects. Fuel 2016, 166, 276.

(13) Meng, F.; Li, X.; Li, M.; Cui, X.; Li, Z. Catalytic Performance of CO Methanation over La-promoted Ni/Al_2O_3 Catalyst in a Slurry-bed Reactor. Chem. Eng. J. 2017, 313, 1548.

(14) Kopyscinski, J.; Schildhauer, T. J.; Biollaz, S. M. A. Production of Synthetic Natural Gas (SNG) from Coal and Dry Biomass − A Technology Review from 1950 to 2009. Fuel 2010, 89, 1763.

(15) Wang, T.; Wang, J.; Jin, Y. Slurry Reactors for Gas-to-Liquid Processes: A Review. Ind. Eng. Chem. Res. 2007, 46, 5824.

(16) Meng, F.; Li, Z.; Liu, J.; Cui, X.; Zheng, H. Effect of Promoter Ce on the Structure and Catalytic Performance of Ni/Al_2O_3 Catalyst for CO Methanation in Slurry-bed reactor. J. Nat. Gas Sci. Eng. 2015, 23, 250.

(17) Götz, M.; Lefebvre, J.; Mörs, F.; McDaniel Koch, A.; Graf, F.; Bajohr, S.; Reimert, R.; Kolb, T. Renewable Power-to-Gas: A technological and Economic Review. Renew. Renewable Energy 2016, 85, 1371.

(18) Todic, B.; Bhatelia, T.; Froment, G. F.; Ma, W.; Jacobs, G.; Davis, B. H.; Bukur, D. B. Kinetic Model of Fischer−Tropsch

Synthesis in a Slurry Reactor on Co−Re/Al_2O_3 Catalyst. Ind. Eng. Chem. Res. 2013, 52, 669.
(19) Zhang, J.; Bai, Y.; Zhang, Q.; Wang, X.; Zhang, T.; Tan, Y.; Han, Y. Low-temperature Methanation of Syngas in Slurry Phase over Zr-doped Ni/γ-Al_2O_3 Catalysts Prepared using Different Methods. Fuel 2014, 132, 211.
(20) Lefebvre, J.; Götz, M.; Bajohr, S.; Reimert, R.; Kolb, T. Improvement of Three-phase Methanation Reactor Performance for Steady-state and Transient Operation. Fuel Process. Technol. 2015, 132, 83.
(21) Götz, M.; Lefebvre, J.; Mörs, F.; Reimert, R.; Graf, F.; Kolb, T. Hydrodynamics of Organic and Ionic Liquids in a Slurry Bubble Column Reactor Operated at Elevated Temperatures. Chem. Eng. J. 2016, 286, 348.
(22) Gao, Y.; Meng, F.; Cheng, Y.; Li, Z. Influence of Fuel Additives in the Urea-nitrates Solution Combustion Synthesis of Ni-Al_2O_3 Catalyst for Slurry Phase CO Methanation. Appl. Catal., A 2017, 534, 12.
(23) Zhang, J.; Xin, Z.; Meng, X.; Lv, Y.; Tao, M. Effect of MoO_3 on Structures and Properties of Ni-SiO_2 Methanation Catalysts Prepared by the Hydrothermal Synthesis Method. Ind. Eng. Chem. Res. 2013, 52, 14533.
(24) Liu, Q.; Gu, F.; Lu, X.; Liu, Y.; Li, H.; Zhong, Z.; Xu, G.; Su, F. Enhanced Catalytic Performances of Ni/Al_2O_3 Catalyst via Addition of V_2O_3 for CO Methanation. Appl. Catal., A 2014, 488, 37.
(25) Tan, M.; Wang, X.; Wang, X.; Zou, X.; Ding, W.; Lu, X. Influence of Calcination Temperature on Textural and Structural Properties, Reducibility, and Catalytic Behavior of Mesoporous γ-alumina-supported Ni−Mg Oxides by One-pot Template-free Route. J. Catal. 2015, 329, 151.
(26) Gao, Y.; Meng, F.; Li, X.; Wen, J.; Li, Z. Factors Controlling Nanosized Ni-Al_2O_3 Catalysts Synthesized by Solution Combustion for Slurry-phase CO Methanation: The Ratio of Reducing Valences to Oxidizing Valences in Redox Systems. Catal. Sci. Technol. 2016, 6, 7800.
(27) Takenaka, S.; Shimizu, T.; Otsuka, K. Complete Removal of Carbon Monoxide in Hydrogen-rich Gas Stream Through Methana-tion over Supported Metal Catalysts. Int. J. Hydrogen Energy 2004, 29, 1065.
(28) da Silva, D. C. D.; Letichevsky, S.; Borges, L. E. P.; Appel, L. G. The Ni/ZrO_2 Catalyst and the Methanation of CO and CO_2. Int. J. Hydrogen Energy 2012, 37, 8923.
(29) Meng, F.; Li, Z.; Ji, F.; Li, M. Effect of ZrO_2 on Catalyst Structure and Catalytic Methanation Performance over Ni-based Catalyst in Slurry-bed Reactor. Int. J. Hydrogen Energy 2015, 40, 8833.
(30) Wang, Y.; Wu, R.; Zhao, Y. Effect of ZrO_2 Promoter on Structure and Catalytic Activity of the Ni/SiO_2 Catalyst for CO Methanation in Hydrogen-rich Gases. Catal. Today 2010, 158, 470.
(31) Liu, D.; Wang, Y.; Shi, D.; Jia, X.; Wang, X.; Borgna, A.; Lau, R.; Yang, Y. Methane Reforming with Carbon Dioxide over a Ni/ZiO_2− SiO_2 Catalyst: Influence of Pretreatment Gas Atmospheres. Int. J. Hydrogen Energy 2012, 37, 10135.
(32) Xu, L.; Zhao, H.; Song, H.; Chou, L. Ordered Mesoporous Alumina Supported Nickel Based Catalysts for Carbon Dioxide Reforming of Methane. Int. J. Hydrogen Energy 2012, 37, 7497.
(33) Tao, M.; Meng, X.; Xin, Z.; Bian, Z.; Lv, Y.; Gu, J. Synthesis and Characterization of Well Dispersed Nickel-incorporated SBA-15 and its High Activity in Syngas Methanation Reaction. Appl. Catal., A 2016, 516, 127.
(34) Kim, D. H.; Sim, J. K.; Lee, J.; Seo, H. O.; Jeong, M.-G.; Kim, Y. D.; Kim, S. H. Carbon Dioxide Reforming of Methane over Mesoporous Ni/SiO_2. Fuel 2013, 112, 111.
(35) Aziz, M. A. A.; Jalil, A. A.; Triwahyono, S.; Mukti, R. R.; Taufiq-Yap, Y. H.; Sazegar, M. R. Highly Active Ni-promoted Mesostructured Silica Nanoparticles for CO_2 Methanation. Appl. Catal., B 2014, 147, 359.
(36) Li, P.; Zhu, M.; Dan, J.; Kang, L.; Lai, L.; Cai, X.; Zhang, J.; Yu, F.; Tian, Z.; Dai, B. Two-dimensional Porous SiO_2 Nanomesh Supported High Dispersed Ni Nanoparticles for CO Methanation. Chem. Eng. J. 2017, 326, 774.
(37) Wang, L.; Zhang, J.; Yang, S.; Sun, Q.; Zhu, L.; Wu, Q.; Zhang, H.; Meng, X.; Xiao, F. Sulfonated Hollow Sphere Carbon as an Efficient Catalyst for Acetalisation of Glycerol. J. Mater. Chem. A 2013, 1, 9422.
(38) Lucchini, M. A.; Testino, A.; Kambolis, A.; Proff, C.; Ludwig, C. Sintering and Coking Resistant Core−shell Microporous Silica−nickel Nanoparticles for CO Methanation: Towards Advanced Catalysts Production. Appl. Catal., B 2016, 182, 94.
(39) Cao, A.; Lu, R.; Veser, G. Stabilizing Metal Nanoparticles for Heterogeneous Catalysis. Phys. Chem. Chem. Phys. 2010, 12, 13499.
(40) Li, S.; Gong, J. Strategies for Improving the Performance and Stability of Ni-based Catalysts for Reforming Reactions. Chem. Chem. Soc. Rev. 2014, 43, 7245.
(41) Wang, X.; Liu, Q.; Jiang, J.; Jin, G.; Li, H.; Gu, F.; Xu, G.; Zhong, Z.; Su, F. SiO_2-stabilized Ni/t-ZrO_2 Catalysts with Ordered Mesopores: one-pot Synthesis and their Superior Catalytic Performance in CO Methanation. Catal. Sci. Technol. 2016, 6, 3529.
(42) Cheng, K.; Subramanian, V.; Carvalho, A.; Ordomsky, V. V.; Wang, Y.; Khodakov, A. Y. The Role of Carbon Pre-coating for the Synthesis of Highly Efficient Cobalt Catalysts for Fischer−Tropsch Synthesis. J. Catal. 2016, 337, 260.
(43) Zhan, W.; He, Q.; Liu, X.; Guo, Y.; Wang, Y.; Wang, L.; Guo, Y.; Borisevich, A. Y.; Zhang, J.; Lu, G.; Dai, S. A Sacrificial Coating Strategy Toward Enhancement of Metal−Support Interaction for Ultrastable Au Nanocatalysts. J. Am. Chem. Soc. 2016, 138, 16130.
(44) Li, X.; Meng, F.; Cheng, Y.; Gao, Y.; Li, Z. Catalytic Methanation in a Slurry-bed Reactor over Ni/SiO_2 Catalysts: Improvement by ZrO_2 and β-cyclodextrin Addition. React. Kinet., Mech. Catal. 2017, 122, 525.
(45) Gao, Y.; Meng, F.; Ji, K.; Song, Y.; Li, Z. Slurry Phase Methanation of Carbon Monoxide over Nanosized Ni−Al_2O_3 Catalysts Prepared by Microwave-assisted Solution Combustion. Appl. Catal., A 2016, 510, 74.
(46) Varma, A.; Mukasyan, A. S.; Rogachev, A. S.; Manukyan, K. V. Solution Combustion Synthesis of Nanoscale Materials. Chem. Rev. 2016, 116, 14493.
(47) Wojcieszak, R.; Monteverdi, S.; Mercy, M.; Nowak, I.; Ziolek, M.; Bettahar, M. M. Nickel Containing MCM-41 and AlMCM-41 Mesoporous Molecular Sieves. Appl. Catal., A 2004, 268, 241.
(48) Seo, J. G.; Youn, M. H.; Song, I. K. Effect of SiO_2-ZrO_2 Supports Prepared by a Grafting Method on Hydrogen Production by Steam Reforming of Liquefied Natural Gas over Ni/SiO_2-ZrO_2 Catalysts. J. Power Sources 2007, 168, 251.
(49) Tao, M.; Meng, X.; Lv, Y.; Bian, Z.; Xin, Z. Effect of Impregnation Solvent on Ni Dispersion and Catalytic Properties of Ni/SBA-15 for CO Methanation Reaction. Fuel 2016, 165, 289.
(50) Zeng, Y.; Ma, H.; Zhang, H.; Ying, W.; Fang, D. Highly Efficient $NiAl_2O_4$-free Ni/γ-Al_2O_3 Catalysts Prepared by Solution Combustion Method for CO Methanation. Fuel 2014, 137, 155.
(51) Liu, Q.; Liu, Z.; Liao, L.; Dong, X. Selective CO Methanation over Amorphous Ni-Ru-B/ZrO_2 Catalyst for Hydrogen-rich Gas Purification. J. Nat. Gas Chem. 2010, 19, 497.
(52) Li, Z.; Meng, F.; Ren, J.; Zheng, H.; Xie, K. Surface Structure and Catalytic Performance of CuCl/SiO_2-Al_2O_3 Catalysts for Methanol Oxidative Carbonylation. Chinese J. Catal. 2008, 29, 643.
(53) Munnik, P.; de Jongh, P. E.; de Jong, K. P. Recent Developments in the Synthesis of Supported Catalysts. Chem. Rev. 2015, 115, 6687.
(54) Meng, F.; Song, Y.; Li, X.; Cheng, Y.; Li, Z. Catalytic Methanation Performance in a Low-temperature Slurry-bed Reactor over Ni−ZrO_2 Catalyst: Effect of the Preparation Method. J. Sol-Gel Sci. Technol. 2016, 80, 759.
(55) Sietsma, J. R. A.; Meeldijk, J. D.; Versluijs-Helder, M.; Broersma, A.; Dillen, A. J. v.; de Jongh, P. E.; de Jong, K. P. Ordered Mesoporous Silica to Study the Preparation of Ni/SiO_2 ex Nitrate Catalysts: Impregnation, Drying, and Thermal Treatments. Chem. Mater. 2008, 20, 2921.